

High $p\text{CO}_2$ reduces sensitivity to CO_2 perturbations on temperate, Earth-like planets throughout most of habitable zone

R.J. Graham

Atmospheric, Oceanic, and Planetary Physics, Clarendon Laboratory, Department of Physics,
University of Oxford, Oxford OX1 3PU, UK

Running Title: Climate stability on high- $p\text{CO}_2$ planets

Keywords: Habitability, astrobiology, planetary climate, extinctions

Submitted November 30, 2020

Reviews received March 23rd, 2021

Resubmitted April 2, 2021

Abstract

The nearly logarithmic radiative impact of CO₂ means that planets near the outer edge of the liquid water habitable zone (HZ) require $\sim 10^6$ x more CO₂ to maintain temperatures conducive to standing liquid water on the planetary surface than their counterparts near the inner edge. This logarithmic radiative response also means that atmospheric CO₂ changes of a given mass will have smaller temperature effects on higher pCO₂ planets. Ocean pH is linked to atmospheric pCO₂ through seawater carbonate speciation and calcium carbonate dissolution/precipitation, and the response of pH to changes in pCO₂ also decreases at higher initial pCO₂. Here, we use idealized climate and ocean chemistry models to demonstrate that CO₂ perturbations large enough to cause catastrophic changes to surface temperature and ocean pH on low-pCO₂ planets in the innermost region of the HZ are likely to have much smaller effects on planets with higher pCO₂. Major bouts of extraterrestrial fossil fuel combustion or volcanic CO₂ outgassing on high-pCO₂ planets in the mid-to-outer HZ should have mild or negligible impacts on surface temperature and ocean pH. Owing to low pCO₂, Phanerozoic Earth's surface environment may be unusually volatile compared to similar planets receiving lower insolation.

1. Introduction

Transient perturbations to the carbon cycle that draw down or release large quantities of CO₂ are known to have played a central role in Earth's climatic history and the evolution of life. Many of the major and minor extinction events of the Phanerozoic Eon are thought to have been caused in part by global heating and ocean acidification from the CO₂ spewed by the eruptions of massive volcanic systems called large igneous provinces (LIPs) [Kidder & Worsley (2010), Sobolev et al. (2011), Bond & Wignall (2014), Bond & Grasby (2017), Ernst & Youbi (2017)]. The most extreme known example of this phenomenon is the Permian-Triassic extinction, which wiped out up to 96% of marine species and likely resulted from the eruption of the Siberian Traps LIP through a large organic carbon deposit [Benton (2018)]. Conversely, cooling periods throughout the Phanerozoic have been driven by tropical

arc-continent collisions and flood basalt eruptions, each of which can trigger CO₂ drawdown by exposing fresh silicates to the surface that are subsequently weathered [Ernst & Youbi (2017), Macdonald et al. (2019)]. Pulses of CO₂ consumption may also have served as triggers or preconditions for one or more of the Snowball Earth glaciations that occurred at the ends of the Archean and Proterozoic eons [Donnadieu et al. (2004), Cox et al. (2016), Somelar et al. (2020)]. Furthermore, ongoing anthropogenic CO₂ emission is comparable to that of other major carbon release events during the Phanerozoic [Foster et al. (2018)], though much more rapid, and the consequences for human civilization and the biosphere would be severe if the flood of CO₂ were allowed to continue until depletion of all fossil fuel resources [Ramirez et al. (2014)].

The above helps make it clear that the Earth's habitability is fundamentally influenced – in some cases, threatened— by large, rapid carbon cycle perturbations [Rothman (2017)]. This motivates a broader analysis of these events to understand their potential importance for the habitability of Earth-like planets in general. Are failed Earths that were heated or frozen by CO₂ perturbations until sterilized of complex life common in the galaxy?

On Earth, the sequestration of CO₂ by the temperature-dependent chemical conversion of silicate minerals on the continents and seafloor into carbonate minerals is thought to have acted as a first-order negative feedback on climate over geologic timescales [Walker et al. (1981), Coogan & Gillis (2013), Maher & Chamberlain (2014), Graham & Pierrehumbert (2020)]. Under a cooling trend, silicate weathering slows down, allowing CO₂ from volcanic outgassing to build to higher levels and oppose the cooling, and the opposite happens in response to warming. This stabilizing feedback modulates climate on 10⁵ - 10⁶ year time intervals [Colbourn et al. (2015)]. Control of CO₂ partial pressure via the silicate weathering feedback is likely a primary reason the planet has remained habitable for the past 4 billion years (Ga) [Walker et al. (1981)], despite an initial solar luminosity of about 70% of its modern value and a $(1-0.7)/0.7 \approx 40\%$ increase in luminosity over the same period [Sagan & Mullen (1972), Charnay et al. (2020)]. When the sun was dimmer, pCO₂ was higher because

of the feedback, and the increase in solar brightness has been slow enough for weathering to draw down CO₂ and maintain climate in a quasi-steady-state with respect to evolving luminosity.

A working hypothesis that underlies the concept of the classical habitable zone (HZ) (the circumstellar region where N₂-CO₂-H₂O atmospheres can provide enough warming to maintain stable surface liquid water) is that at least some Earth-like exoplanets within the HZ of their stars can support a silicate weathering feedback like Earth's [Kasting et al. (1988), Kasting et al. (1993), Kopparapu et al. (2013)]. This would imply that this subpopulation of rocky planets will display a trend in pCO₂ vs. incoming stellar radiation ("instellation"), with planets that receive less instellation within the HZ generally building up thicker pCO₂ atmospheres to compensate for the cooling at lower luminosity [Bean et al. (2017)]. This would allow for the maintenance of liquid water on the surfaces of Earth-like planets for longer periods of time and over a much wider range of conditions than would otherwise be likely.

The radiative forcing response to CO₂ is approximately logarithmic, meaning a progressively larger CO₂ change is required in order to produce a given amount of forcing as the background CO₂ level increases [Pierrehumbert (2010), Huang & Bani Shahabadi (2014)] (the deviation from logarithmic behavior at high pCO₂ due to self-broadening does not materially affect this point, see e.g. Fig. 1). This means that the pCO₂ required to maintain surface temperatures above freezing rises rapidly as instellation falls, going from parts per million of a bar in the inner portion of the HZ to bars or tens of bars in the mid-to-outer reaches. Given this huge gradient in pCO₂ for N₂-CO₂-H₂O atmospheres across the HZ, changes in CO₂ that might cause catastrophe in the inner-HZ should have much smaller impacts in the outer-HZ because of the logarithmic forcing effect. For example, a LIP that suddenly increased the atmospheric CO₂ concentration on an inner-HZ planet from a few hundred parts per million by volume (ppmv) to a few thousand ppmv would likely cause severe warming and (in the presence of life) a mass extinction, but adding the same mass of CO₂ to an atmosphere in the outer-HZ that already had a pCO₂ of a few bars would result in a negligible change in surface temperature.

In this article, we use an idealized climate model to quantify the variation in temperature impact of transient carbon perturbations to the atmospheres of Earth-like planets with different $p\text{CO}_2$ values at a range of instellations throughout the HZ. We also apply a basic model of carbonate equilibrium and calcium carbonate buffering in the sea to estimate the extent of ocean acidification from these perturbations, another of the important killing mechanisms in mass extinctions caused by LIPs on Earth [Benton (2018)]. In Section 2, we introduce the models used in the article. In Section 3, we present the results of the calculations, demonstrating extreme climate resilience to carbon cycle perturbations for temperate planets in the mid-to-outer reaches of the HZ. In section 4, we discuss caveats and implications of these results, and in section 5 we summarize and conclude the study.

2. Modeling & Methods

2.1. Energy balance climate model

To investigate the climate sensitivity of Earth-like planetary climate to carbon cycle perturbations at varying instellations, we examine the changes to global-mean surface temperature from atmospheric CO_2 increases equivalent to 5000 gigatonnes of carbon (GtC) and 50,000 GtC. A perturbation of 5000 GtC is on the order of the size of perturbation that caused the Paleocene-Eocene Thermal Maximum [McInerney & Wing (2011)] and is approximately equal to estimates of total global hydrocarbon resources (which includes both accessible and currently-inaccessible reservoirs of fossil fuels) [Rogner (1997), Ramirez et al. (2014)]. A perturbation of 50,000 GtC is of the same order of magnitude as the carbon release caused by the Siberian Traps during the Permian-Triassic mass extinction [Svensen et al. (2009)]. We use an “inverse climate modeling” approach, as described in e.g. [Kasting (1991)], to calculate the initial pre-perturbation climate in each case: the surface temperature and $p\text{CO}_2$ are first assumed, which allows calculation of the albedo and outgoing longwave radiation (OLR), which can together be used to calculate the effective stellar flux (S_{eff} ; the ratio of incoming stellar flux, S , on a given planet to modern Earth’s insolation of $S_{\text{earth}}=1368 \text{ W m}^{-2}$)

required to sustain the assumed global-mean temperature-pCO₂ combination under the assumption of global-mean energy balance:

$$S_{\text{eff}} = \frac{S}{S_{\text{earth}}} = \frac{4 \times OLR(T, p\text{CO}_2)}{S_{\text{earth}} \times (1 - a(T, p\text{CO}_2))} \quad (1)$$

where $a(T, p\text{CO}_2)$ is the planetary albedo and all other symbols have been introduced above. This highly idealized, global-mean approach is justified for this study because the climate effect we demonstrate results from the basic, qualitative behavior of atmospheric CO₂.

To calculate OLR as a function of pCO₂ and global-mean surface temperature, we apply a piecewise 6th-degree polynomial function developed by [Kadoya & Tajika (2019)] to approximate simulations of an N₂-CO₂-H₂O atmosphere by the 1D radiative-convective column model used in [Haqq-Misra et al. (2016)]. The fit can accurately (with error <=3.3 W m⁻²) reproduce the column model's OLR output for 10⁻⁵ bar < pCO₂<10 bar and 150 K < T < 350 K. For all pCO₂ and T, the atmosphere has a constant pN₂ = 1 bar and is saturated with H₂O. OLR output from this model is plotted as a function of temperature over the range 273 K < T < 340 K and pCO₂ over the range 10⁻⁴ bar < pCO₂ < 10 bar in Fig. 1. In matrix form, the equation is:

$$OLR(T, p\text{CO}_2) = I_0 + \mathbf{T}\mathbf{B}\mathbf{Y}^t \quad (2)$$

$$\mathbf{T} = (1 \ \xi \ \xi^2 \ \xi^3 \ \xi^4 \ \xi^5 \ \xi^6) \quad (3)$$

$$\mathbf{Y} = (1 \ v \ v^2 \ v^3 \ v^4) \quad (4)$$

where T is the surface temperature in Kelvin, pCO₂ is the partial pressure of CO₂ in bars, and $\xi = 0.01x(T-250)$. For pCO₂ < 1 bar,

$$p = 0.2 \times \log_{10}(p\text{CO}_2) \quad (5)$$

$$\mathbf{B} = \begin{bmatrix} 87.8373 & -311.289 & -504.408 & -422.929 & -134.611 \\ 54.9102 & -677.741 & -1440.63 & -1467.04 & -543.371 \\ 24.7875 & 31.3614 & -364.617 & -747.352 & -395.401 \\ 75.8917 & 816.426 & 1565.03 & 1453.73 & 476.475 \\ 43.0076 & 339.957 & 996.723 & 1361.41 & 612.967 \\ -31.4994 & -261.362 & -395.106 & -261.600 & -36.6589 \\ -28.8846 & -174.942 & -378.436 & -445.878 & -178.948 \end{bmatrix} \quad (6)$$

and when $p\text{CO}_2$ exceeds 1 bar, p and \mathbf{B} are instead:

$$p = \log_{10}(p\text{CO}_2) \quad (7)$$

$$\mathbf{B} = \begin{bmatrix} 87.8373 & -52.1056 & 35.2800 & -1.64935 & -3.43858 \\ 54.9102 & -49.6404 & -93.8576 & 130.671 & -41.1725 \\ 24.7875 & 94.7348 & -252.996 & 171.685 & -34.7665 \\ 75.8917 & -180.679 & 385.989 & -344.020 & 101.455 \\ 43.0076 & -327.589 & 523.212 & -351.086 & 81.0478 \\ -31.4994 & 235.321 & -462.453 & 346.483 & -90.0657 \\ -28.8846 & 284.233 & -469.600 & 311.854 & -72.4874 \end{bmatrix} \quad (8)$$

with symbols retaining their previous meanings. OLR is plotted as a function of temperature over the range $273 \text{ K} < T < 340 \text{ K}$ and $p\text{CO}_2$ over the range $10^{-4} \text{ bar} < p\text{CO}_2 < 10 \text{ bar}$ in Fig. 1.

We calculate global-mean planetary albedo using another polynomial fit to radiative-convective model output for a planet orbiting a Sun-like star with $T_{\text{eff}}=5800 \text{ K}$, sourced from the same model the OLR equation is fit to, though in this case the albedo parameterization comes from [Haqq-Misra et al. (2016)]:

$$\begin{aligned} \alpha(t, a_s, \mu, \phi) = & A\mu^3 + B\mu^2 a_s + C\mu^2 t + D\mu^2 \phi + E\mu^2 + F\mu a_s^2 + G\mu a_s t + H\mu a_s \phi \\ & + I\mu a_s + J\mu t^2 + K\mu t \phi + L\mu t + M\mu \phi^2 + N\mu \phi + O\mu + P a_s^3 \\ & + Q a_s^2 t + R a_s^2 \phi + S a_s^2 + T_0 a_s t^2 + U a_s t \phi + V a_s t + W a_s \phi^2 \\ & + X a_s \phi + Y a_s + Z t^3 + A A t^2 \phi + A B t^2 + A C t \phi^2 + A D t \phi + A E t \\ & + A F \phi^3 + A G \phi^2 + A H \phi + A G \end{aligned} \quad (9)$$

where $t = \log_{10}(T)$, a_s is the surface albedo (taken to be 0.3 by default), μ is the cosine of the stellar zenith angle (taken to be $2/3$, the instellation-weighted average, following [Cronin (2014)]), and $\phi = \log_{10}(p\text{CO}_2)$. The coefficients A through AG in the equation can be downloaded as a [tar.gz](#) file made available by Haqq-Misra et al. The file includes coefficients for stars with stellar effective temperatures of 3400 K, 4600 K, 5800 K (which we use), and 7200 K, since different stellar spectra lead to different planetary albedos. The coefficient values are also listed in Table 1.

Table 1: The coefficients in Eq. (9) for albedo

Label	Coefficient value	Label	Coefficient value
A	-4.41391620e-01	S	6.11699085e-01
B	-2.60017516e-01	T_0	-2.33213410e+00
C	1.08110772e+00	U	2.56011431e-01
D	-3.93863286e-02	V	1.05912148e+01
E	-1.46383456e+00	W	-1.85772689e-02
F	9.91383779e-02	X	-7.55796861e-01
G	-1.45914724e+00	Y	-1.16485004e+01
H	-2.72769393e-02	Z	2.74062492e+01
I	3.99933641e+00	AA	5.46044241e-01
J	1.07231336e+00	AB	-2.05761674e+02
K	-1.04302521e-02	AC	5.57943359e-02
L	-6.10296439e+00	AD	-2.49880330e+00
M	2.69255204e-03	AE	5.14448995e+02
N	9.50143253e-02	AF	2.43702089e-03
O	7.37864216e+00	AG	-1.09384841e-01
P	1.28580729e-01	AH	2.92643187e+00
Q	-3.07800301e-01	AG	-4.27802455e+02
R	2.27715595e-02		

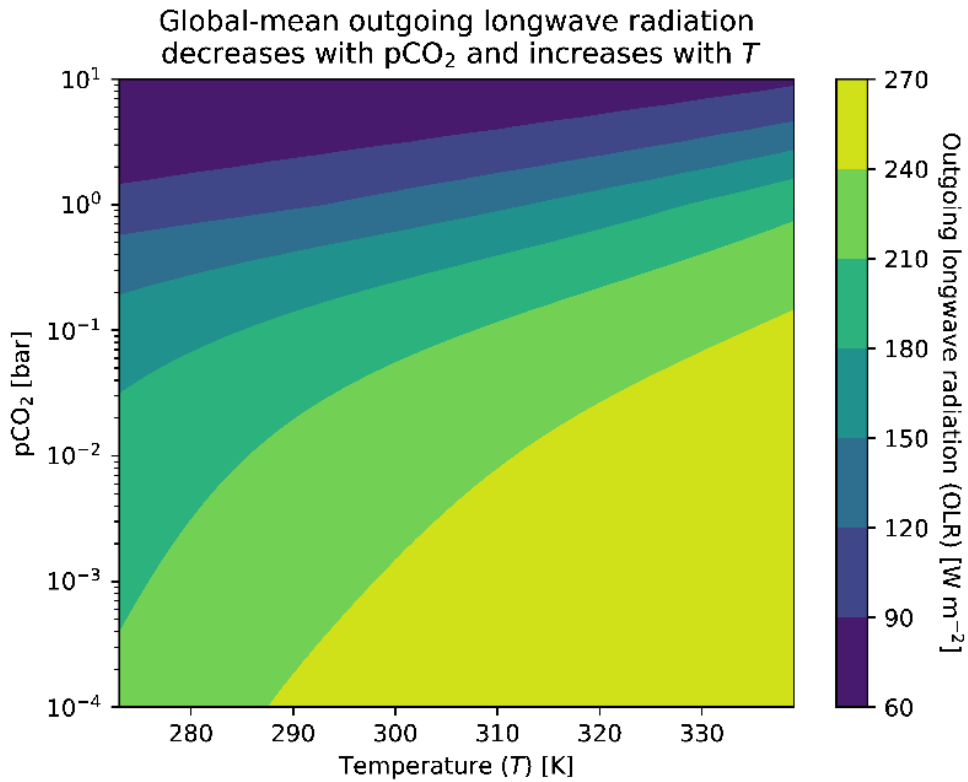


Fig. 1: OLR as a function of $p\text{CO}_2$ and global-mean surface temperature T .

Increasing $p\text{CO}_2$ elevates albedo due to CO_2 's strong Rayleigh scattering cross-section, and increasing temperature tends to reduce albedo by increasing the concentration of H_2O , which absorbs longwave and some shortwave radiation, reducing the effectiveness of scattering. Albedo is plotted as a function of temperature over global-mean surface temperature range $273 \text{ K} < T < 340 \text{ K}$ and $p\text{CO}_2$ range $10^{-4} \text{ bar} < p\text{CO}_2 < 10 \text{ bar}$ in Fig. 2. The slight reduction in albedo visible in Fig. 2 that occurs with a $p\text{CO}_2$ increase from 10^{-4} bar to 10^{-3} bar at a temperature of around 325 K is a spurious result of an imperfect polynomial fit, but the simulations in this study never access that region of the parameter space, so it does not impact the results presented here.

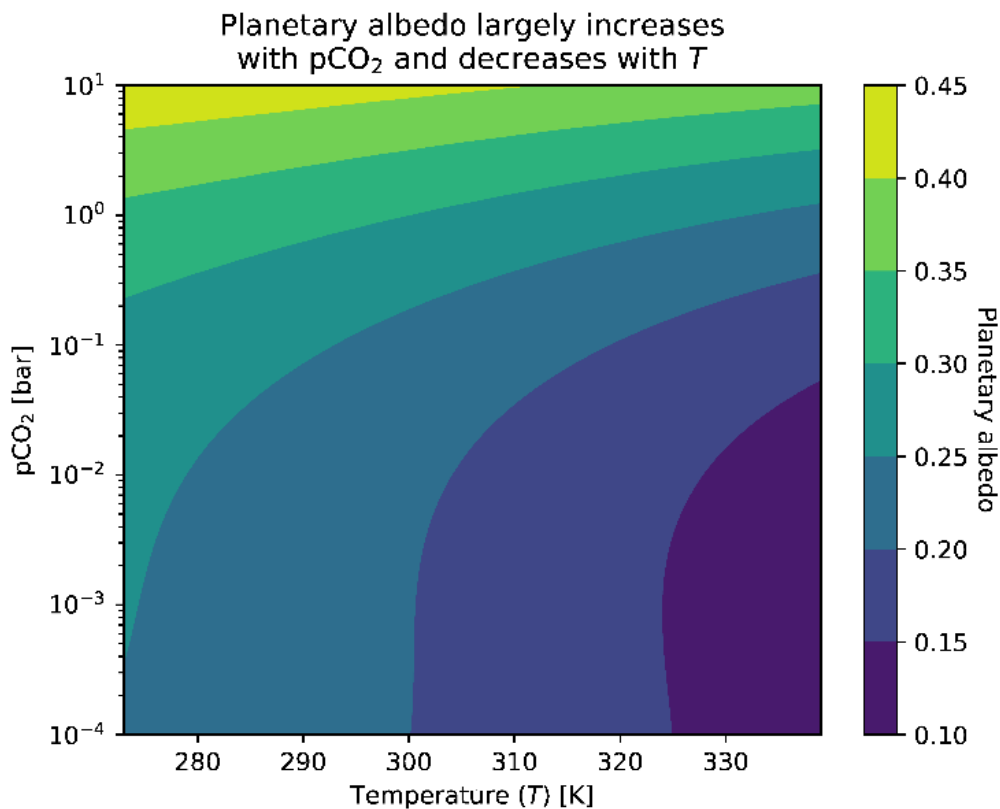


Fig. 2: Planetary albedo as a function of $p\text{CO}_2$ and global-mean surface temperature T .

With boundary conditions characteristic of pre-industrial Earth, e.g. an instellation of $S = 1368 \text{ W m}^{-2}$ and $p\text{CO}_2 = 280 \times 10^{-6} \text{ bar}$, the model produces $T = 309 \text{ K}$, significantly hotter than Earth's pre-industrial temperature of $\sim 285 \text{ K}$ [Walker et al. (1981)]. This is at least partly because the model

atmosphere is assumed to be saturated with water vapor, whereas Earth's atmosphere is held at global-mean relative humidities less than 1 due to regions of dry, subsiding air, allowing for more efficient radiation to space and thus cooler surface temperatures e.g. [Pierrehumbert (1995)]. In addition, cloud feedbacks that can have important impacts on OLR and albedo are not included in this model. Cloud effects can alter long term climate and the relationship between $p\text{CO}_2$ and temperature at a given instellation on Earth-like planets e.g. [Goldblatt et al. (2021)], but they are intrinsically 3-dimensional phenomena, so they require 3-D general circulation models to simulate. To ensure the simplifications noted above are minor for the purposes of this study, next we evaluate the sensitivity of the climate model to ensure it reproduces the relevant behavior of more sophisticated models.

Equilibrium climate sensitivity (ECS) tends to increase with CO_2 until the albedo increase from Rayleigh scattering by CO_2 begins to compete with the greenhouse effect

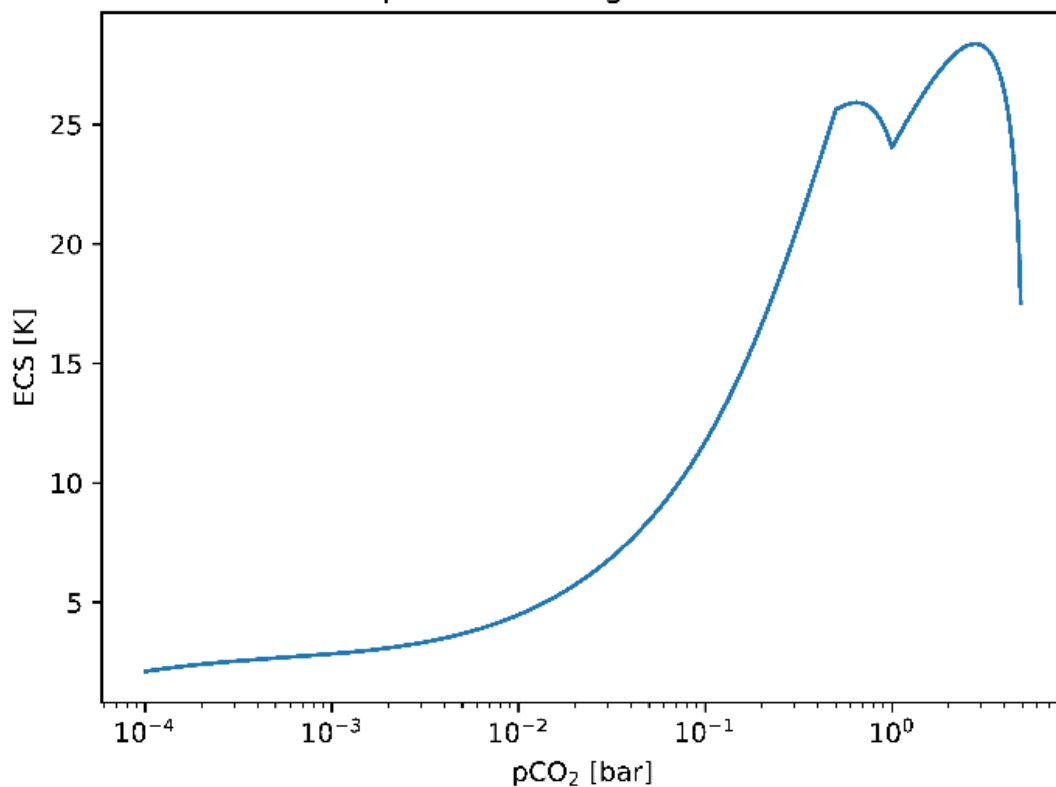


Fig. 3: ECS as a function of $p\text{CO}_2$ for planets with initial $T=273.15$ K.

The steady-state global-mean temperature increase produced by a doubling of CO_2 is known as the equilibrium climate sensitivity (ECS) and is a common metric in studies of Earth climate. In more sophisticated climate models than the model used in this paper, the value of ECS is dependent on many processes in addition to the radiative effects of CO_2 (and H_2O), particularly the dynamics of low-lying, high-albedo clouds [Wolf et al. (2018), Schneider et al. (2019)]. Based on climate models of varying complexity, ECS on Earth may vary by an order of magnitude depending on background conditions, from ~ 2 K to ~ 20 K, with a general trend toward higher sensitivity as $p\text{CO}_2$ increases and a pronounced maximum at warm temperatures and intermediate $p\text{CO}_2$ that arises from low-lying cloud dissipation [Wolf et al. (2018)] and clear-sky radiative feedbacks [Seeley & Jeevanjee (2020)]. To ensure that the model in this paper produces reasonable climatic responses to CO_2 changes, we examine the temperature perturbations from $p\text{CO}_2$ doublings with initial $p\text{CO}_2$ values ranging from 10^{-4} bar to 5 bars (beyond which a CO_2 doubling takes the model outside of its range of validity in $p\text{CO}_2$ space), with each simulation initialized at $T=273.15$ K (see Fig. 3). The range of ECS values produced by our climate model is broadly consistent with the range of values in the literature (e.g. the ECS throughout Earth history is estimated to have varied between 2.6 K and 21.6 K by [Wolf et al. (2018)]), though there is no maximum at intermediate $p\text{CO}_2$ since the calculations are all carried out with low initial temperatures. The model does reproduce the intermediate- $p\text{CO}_2$ ECS maximum when initialized at $T \geq \sim 300$ K, (not shown). At $p\text{CO}_2 = 10^{-4}$ bar, $\text{ECS} \sim 2$ K, which increases to a maximum of around 27 K near 2 bars. These numbers vary by a few degrees in either direction when the model is initialized from different temperatures, but the differences are small relative to the effects demonstrated in this study. The kink in the ECS that occurs at 1 bar is due to the discontinuity at $p\text{CO}_2 = 1$ bar in the OLR polynomial fit from [Kadoya & Tajika (2019)] used in this climate model. CO_2 's self-broadening increases ECS as background $p\text{CO}_2$ goes up, meaning the model's radiative behavior is not perfectly logarithmic (ECS would be constant in that case), but ECS varies by approximately an order of magnitude across five orders of magnitude of $p\text{CO}_2$, confirming the usefulness of the logarithmic approximation in discussing the model's behavior. ECS begins to decrease rapidly beyond

about 2 bars because of the increasing relative impact of CO₂'s Rayleigh scattering on the energy balance of the planet. If the curve were extended until ECS intercepted the x-axis, that point would define the "maximum greenhouse limit," beyond which the addition of CO₂ to the atmosphere would cool the planet e.g. [Kopparapu et al. (2013)].

We first determine the S_{eff} necessary at a given $p\text{CO}_2$ to hold a planet's global-mean temperature at H₂O's freezing point, $T=273.15$ K, which serves as an approximate minimum temperature & $p\text{CO}_2$ for surface habitability at a given instellation. This is a conservative choice for addressing the question of the impact of carbon cycle perturbations, as it minimizes initial atmospheric CO₂, maximizing the impact of a given $p\text{CO}_2$ increase. Then, given the initial CO₂, we calculate the $p\text{CO}_2$ increase from the addition of a mass of CO₂ m_{CO_2} :

$$\Delta p\text{CO}_2 = \frac{\mu_{\text{atm}}}{\mu_{\text{CO}_2}} \frac{m_{\text{CO}_2} g}{4\pi R_{\text{earth}}^2} \quad (10)$$

where $\Delta p\text{CO}_2$ is the change in CO₂ partial pressure, μ_{atm} , which varies with relative proportions of CO₂ and N₂ ($\mu_{\text{N}_2}=28$ g mol⁻¹), is the molar mass for the atmosphere as a whole, $\mu_{\text{CO}_2}=44$ g mol⁻¹ is the molar mass for CO₂, $g=9.81$ m s⁻² is the acceleration due to gravity on Earth (we assume planets are the same size as Earth in this article), and $R_{\text{earth}}=6.371 \times 10^6$ m is the radius of the Earth. Finally, to calculate the temperature change ΔT from a perturbation, we simply add the $p\text{CO}_2$ increase to the initial $p\text{CO}_2$ and calculate the new temperature necessary to maintain energy balance at the original instellation (S).

2.2. Oceanic carbonate system and pH

To estimate the impact of the calculated changes to $p\text{CO}_2$ and T on seawater pH, we assume the oceanic carbonate system is in equilibrium with atmospheric CO₂ and with calcium carbonate that buffers changes to pH by dissolving or precipitating. The following equations and constants are drawn from [Pierrehumbert (2010)], but with the concentrations converted from units of [mol mol⁻¹] to units of [mol L⁻¹] through multiplication by a factor of 55.56 mol L⁻¹, the number of moles of liquid water

per liter. All constants are set to values appropriate for an ocean depth of 3 km, with salinity approximately equal to 35 grams of salt per kilogram of water. The solubility equilibrium equation for CaCO_3 's dissociation into Ca^{2+} and CO_3^{2-} is:

$$K_{\text{sp}} = [\text{Ca}^{2+}][\text{CO}_3^{2-}] \quad (11)$$

where $K_{\text{sp}} = 7.90 \times 10^{-7} \text{ mol}^2 \text{ L}^{-2}$ is CaCO_3 's solubility product and each bracketed chemical species represents the concentration of that chemical, written as a molarity. The equilibrium equation for the reaction $\text{H}_2\text{O} + \text{CO}_2(\text{aq}) \leftrightarrow \text{H}^+(\text{aq}) + \text{HCO}_3^-(\text{aq})$ can be written:

$$K_1(T) = \frac{[\text{H}^+][\text{HCO}_3^-]}{[\text{CO}_2]} = K_{1,\text{ref}} \times \exp\left(-c_1 \left(\frac{1}{T} - \frac{1}{298}\right)\right) \quad (12)$$

where $K_1(T)$ is the temperature-dependent equilibrium constant, $K_{1,\text{ref}} = 1.32 \times 10^{-6} \text{ mol L}^{-1}$ is the value of K_1 at 298 K, and $c_1 = 1218 \text{ K}$ is the temperature dependence of the reaction. The equilibrium equation for the reaction $\text{HCO}_3^-(\text{aq}) \leftrightarrow \text{H}^+(\text{aq}) + \text{CO}_3^{2-}(\text{aq})$ can be written:

$$K_2(T) = \frac{[\text{H}^+][\text{CO}_3^{2-}]}{[\text{HCO}_3^-]} = K_{2,\text{ref}} \times \exp\left(-c_2 \left(\frac{1}{T} - \frac{1}{298}\right)\right) \quad (13)$$

where the symbols have the same meanings as before (for their respective reaction), $K_{2,\text{ref}} = 8.95 \times 10^{-10} \text{ mol L}^{-1}$, and $c_2 = 2407 \text{ K}$. Henry's law for CO_2 is written:

$$p\text{CO}_2 = k_{\text{H}}[\text{CO}_2] \quad (14)$$

where $k_{\text{H}} = 29 \text{ bar L mol}^{-1}$ is the Henry's law constant for CO_2 , which relates its partial pressure to its concentration in water at equilibrium. Lastly, under the simplifying assumption that Ca^{2+} is the only source of alkalinity in the ocean, charge balance can be written:

$$2[\text{Ca}^{2+}] = [\text{HCO}_3^-] + 2[\text{CO}_3^{2-}] + \frac{10^{-14}}{[\text{H}^+]} - [\text{H}^+] \quad (15)$$

where $\frac{10^{-14}}{[\text{H}^+]}$ is equal to $[\text{OH}^-]$.

Combined and rearranged, the previous five equations produce a convenient fourth degree polynomial relating $[H^+]$ to pCO_2 and T :

$$2K_{sp}[H^+]^4 + \frac{K_1(T)K_2(T)}{k_H} pCO_2[H^+]^3 - \left(\frac{K_1(T)^2 K_2(T)}{k_H^2} pCO_2^2 + \frac{K_1(T)K_2(T)}{k_H} 10^{-14} pCO_2 \right) [H^+] - 2 \frac{K_1(T)^2 K_2(T)^2}{k_H^2} pCO_2^2 = 0 \quad (16)$$

which can be solved for $[H^+]$ (and therefore pH, equal to $-\log_{10}[H^+]$) numerically using the pCO_2 and T output from the climate model. It is worth noting that we are implicitly assuming a higher mass of CO_2 enters the atmosphere-ocean system than m_{CO_2} alone by including ocean carbonate chemistry changes in response to atmospheric CO_2 because some carbon must be diverted into the ocean for changes to pH to occur. This effect becomes smaller as the initial pCO_2 inventory increases farther from the star, since increasing CO_2 causes a larger and larger fraction of the total carbon in the atmosphere-ocean system to be partitioned into the atmosphere [Pierrehumbert (2010)]. With preindustrial Earth-like conditions of $pCO_2 = 280 \times 10^{-6}$ bar and $T = 285$ K, the model produces a pH of 8.32, which is reasonably close to Earth's preindustrial pH of ~ 8.25 [Jacobson (2005)].

3. Results

In Section 3.1, we describe the temperature impact of increases in atmospheric CO_2 of 5000 GtC and 50,000 GtC on planets orbiting G-type stars throughout the HZ. In Section 3.2, we describe the change to oceanic pH from the same CO_2 increases.

3.1. Temperature change from CO_2 perturbations

For both the 5000 GtC perturbation and the 50,000 GtC perturbation, temperature changes go from very large in the inner portion of the HZ to negligibly small in the middle and outer reaches (see middle row of plots in Fig. 4). An initial pCO_2 inventory of 10^{-4} bar is the lowest used in this study, equivalent to a concentration of 100 parts per million by volume (ppmv) of CO_2 in a 1 bar N_2

atmosphere, and this $p\text{CO}_2$ produces an initial $T = 273.15$ K at $S_{\text{eff}}=0.846$. In this case the planet experiences a $p\text{CO}_2$ increase of more than an order of magnitude from the 5000 GtC injection, to 2.3×10^{-3} bar (2300 ppmv; see top-left panel of Fig. 4). This is accompanied by a temperature increase of 15 K (see mid-left panel of Fig. 4). In the 50,000 GtC case, the final $p\text{CO}_2=2.3 \times 10^{-2}$ bar (23,000 ppmv; top-right panel of Fig. 4), with a temperature increase of 36 K (mid-right panel of Fig. 4). For comparison, on Earth, LIP eruptions have been associated with temperature increases of up to 15 K [Ernst & Youbi (2017)].

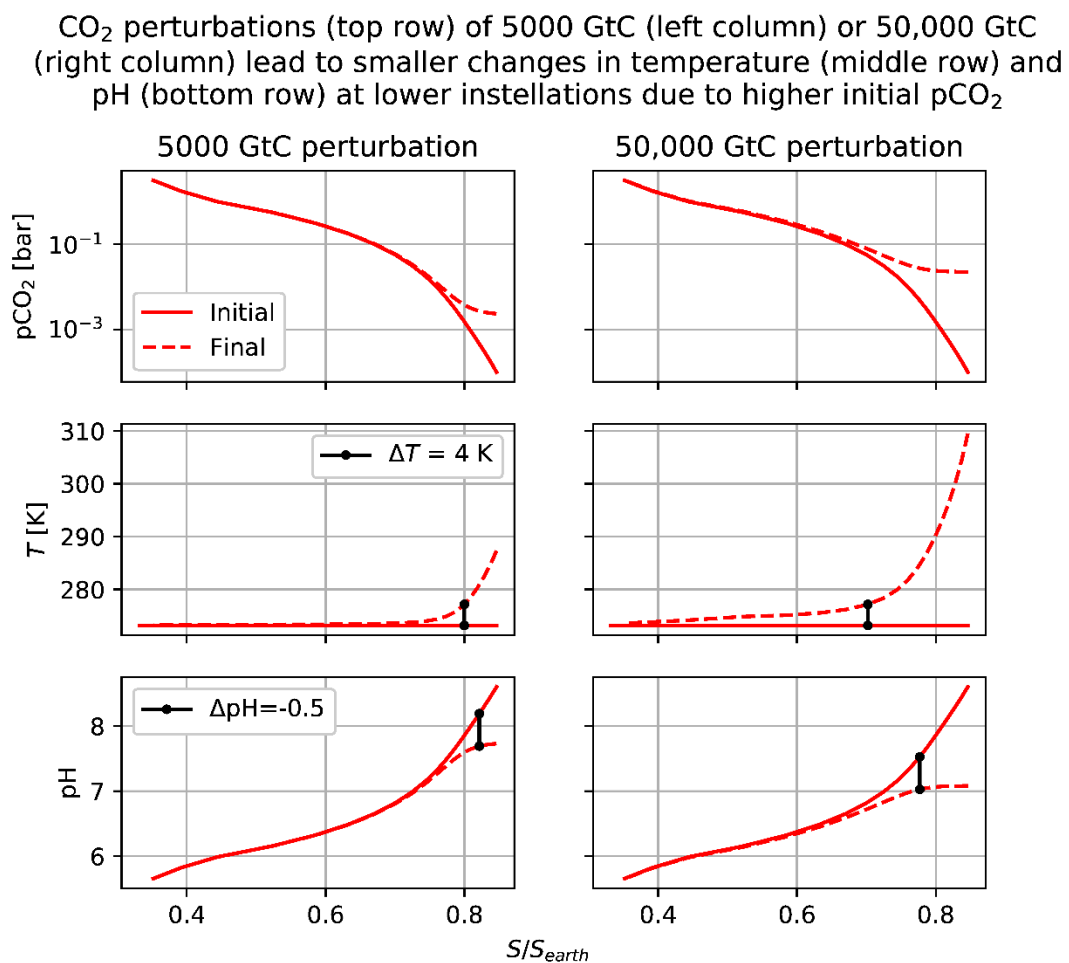


Fig. 4: Comparison of temperature-change and pH-change for CO₂ perturbations of 5000 GtC (left column) and 50,000 GtC (right column). The x-axis in each case is the installation relative to Earth's, $S_{\text{eff}}=S/S_{\text{earth}}$. The top row shows the pre-perturbation (solid curve) and post-perturbation $p\text{CO}_2$ (dashed curve) for planets that are initialized at $T=273.15$ K. The middle row shows the temperature change from the CO₂ perturbations, with the solid and dashed curves representing the pre- and post-perturbation temperature values and the black line segment marking the point where the temperature change falls below 4 K. The bottom row shows the oceanic pH change from the CO₂

perturbations, with the solid and dashed curves representing the pre- and post-perturbation pH values and the black line segment marking where the magnitude of acidification falls below 0.5 pH units.

At the outermost orbit evaluated in this study, S_{eff} is equal to 0.352 and a $p\text{CO}_2$ of 3.162 bars is necessary to initialize at $T=273.15$ K. For that configuration, a 5000 GtC injection elevates $p\text{CO}_2$ to 3.166 bars and increases the temperature by 0.04 K, a change approximately 3 orders of magnitude smaller than the change at the innermost orbit. A 50,000 GtC injection causes a temperature increase of 0.4 K and increases $p\text{CO}_2$ to 3.19 bars.

By choosing a semi-arbitrary level of ΔT as the threshold between a “large” and a “small” climate change, it’s possible to define orbital boundaries beyond which planets inhabit “stability zones” where they experience small changes in response to CO_2 increases of a given size. Here, we use $\Delta T = 4$ K as the threshold value separating large from small, as 4 K of heating by 2100 is a worst-case scenario for anthropogenic climate change which would lead to widespread environmental disaster [New et al. (2011)]. For the 5000 GtC CO_2 injection, $\Delta T \leq 4$ K at $S_{\text{eff}} \leq 0.80$, where the initial $p\text{CO}_2$ was 1.5×10^{-3} bar. For planets orbiting a star with the Sun’s properties where $S_{\text{eff}}=1$ at an orbital radius of 1 astronomical unit (au), this translates to climate stability against 5000 GtC perturbations beyond an orbital distance of $d = \sqrt{1/0.80} = 1.12$ au (see boundary between the orange and yellow rings in Fig. 5). For the 50,000 GtC perturbation, climate stability occurs at $S_{\text{eff}} \leq 0.70$ (with an initial $p\text{CO}_2$ of 5.4×10^{-2} bar), translating to an inner orbital distance of $d = 1.20$ au for the 50,000 GtC stability zone (see boundary between yellow and green rings in top panel of Fig. 5).

The inner edge of the HZ for rapidly-rotating planets is usually defined as the instellation where climates are forced into either a “moist greenhouse” state [Kasting et al. (1984)] or a “runaway greenhouse” state [Ingersoll (1969)], given some assumptions about a planet’s inventory and surface distribution of water. The moist greenhouse state occurs when a planet’s stratosphere becomes wet, triggering efficient photodissociation and hydrogen loss that in time depletes a planet of its oceans [Kasting et al. (1984)]. This can occur at a variety of instellations depending on background $p\text{CO}_2$ and

the atmospheric history of the planet, with values as low as $S_{\text{eff}}=1.03$ to 1.05 recovered in GCM simulations of a rapidly rotating aquaplanet around a Sun-like star [Popp et al. (2016)]. The runaway greenhouse occurs when a planet's absorbed instellation exceeds the maximum OLR the planet can radiate in the presence of a condensed reservoir of greenhouse gas in vapor equilibrium with the atmosphere e.g. [Goldblatt & Watson (2012)], leading to uncontrollable warming until the condensable reservoir has evaporated. The runaway greenhouse limit is about $S = 375 \text{ W m}^{-2}$ for the Sun [Leconte et al. (2013)], which translates to $S_{\text{eff}}=1.1$ and $d = 0.95$ au. As the runaway greenhouse is generally thought to occur closer to the star than the moist greenhouse, we will take the runaway limit as the inner edge of the HZ for our calculations. The outer edge of the HZ, where added CO_2 cools the planet below freezing instead of warming it, is at approximately $d = 1.67$ au in our solar system [Kopparapu et al. (2013)].

With the above choices of inner and outer HZ boundaries, the innermost ring of the HZ where planets are susceptible to both 5000 GtC and 50,000 GtC perturbations has a radial width of 0.17 au, while planets are safe from 5000 GtC perturbations over a 0.55 au range of radii, and planets are safe from both 5000 and 50,000 GtC perturbations across 0.47 au. An alternative visualization of the climate stability is provided in the bottom panels of Fig. 5, which show the temperature responses to the 5000 GtC (bottom-left panel) and 50,000 GtC (bottom-right panel) perturbations as functions of orbital radius. In the 5000 GtC case, the temperature response is less than 1 K throughout most of the HZ, while for the 50,000 GtC perturbation the response is still modest but stays above 1 K until near the outer edge of the HZ. So, throughout most of the classical HZ, temperate planets where CO_2 & H_2O are the dominant greenhouse gases will lie in stability zones where global surface temperature should only be mildly affected by transient carbon cycle perturbations of similar size to those that have repeatedly caused large, catastrophic swings in Earth's surface temperature during the Phanerozoic Eon, and potentially the Neoproterozoic. It is worth noting that if we had assumed a higher initial temperature and a correspondingly higher initial pCO_2 at each luminosity, then the inner boundaries for the stable zones would be even closer to the star, so the choice of initializing at

$T=273.15$ K is conservative. In any case, this calculation is meant to be illustrative; the same qualitative pattern emerges regardless of the choice of T , as long as CO_2 is assumed to be the dominant greenhouse gas offsetting the reduction in solar luminosity with orbital distance.

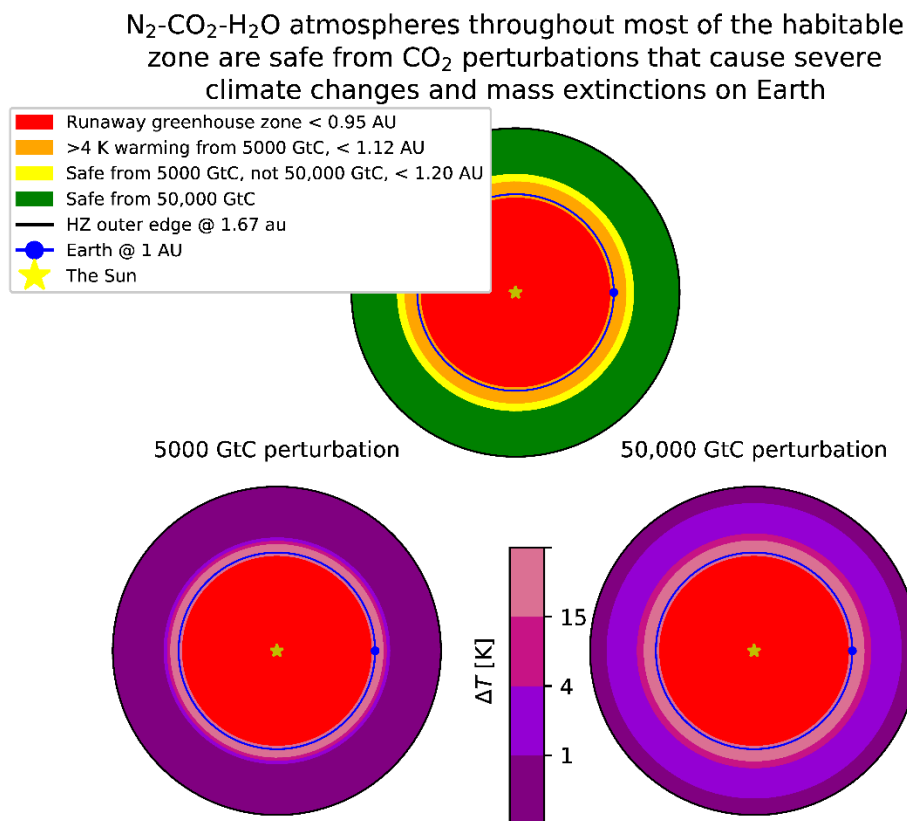


Fig. 5: Illustrations of the climate stability as a function of orbital radius within the habitable zone in a solar system with a star identical to the Sun. The yellow star in the center of each panel represents a Sun-like G-type star. The red zone in each panel is the region where Earth-like planets are likely to be in the uninhabitable runaway greenhouse state, extending to 0.95 au. The circular blue dot and ring in each panel represent the Earth’s orbit, at a radius of 1 au. In the top panel, the orange zone is within the habitable zone but outside of either stability zone, meaning Earth-like planets in this region would have the potential to warm by more than 4 K under a 5000 GtC CO_2 perturbation, based on the temperature response of simulations initialized at $T=273.15$ K. The orange zone extends from the inner edge of the HZ at 0.95 au to 1.12 au. The yellow zone represents the region where planets within the HZ would experience less than 4 K of warming from a 5000 GtC perturbation but more than 4 K of warming from a 50,000 GtC perturbation, and it extends from 1.12 au to 1.20 au. The green zone represents the region where planets within the HZ would experience less than 4 K of warming from either a 5000 GtC perturbation or a 50,000 GtC perturbation, extending from 1.20 au to 1.67 au. The black region is beyond the outer edge of the HZ, beginning at 1.67 au. The bottom panels show the temperature change as a function of orbital radius for the 5000 GtC perturbation (left) and the 50,000 GtC perturbation (right).

3.2. pH change from CO₂ perturbations

Similar to the temperature perturbation results, the change in pH from 5000 and 50,000 GtC atmospheric CO₂ mass injections is large only in the inner region of the HZ (see bottom row in Fig. 4). Initial pH is smaller at lower S_{eff} because of higher initial pCO₂ values. As S_{eff} decreases, so does the reduction in pH from a given CO₂ increase, going from a change of nearly 2 pH units (e.g. a 2 order-of-magnitude increase in [H⁺]) under the 50,000 GtC increase at the innermost orbit to a change of less than one hundredth of a pH unit at the outermost orbit evaluated.

Stability zones for pH can be defined in the same way we defined them for temperature. In this case, we will use -0.5 pH units as the threshold between a “large” and “small” pH change, since that is the estimated level of oceanic pH reduction below the pre-industrial value in the year 2100 for a worst-case scenario of climate change, and represents a level of change that would pose a danger to many extant marine animal taxa [Wittmann & Pörtner (2013)]. With that choice of threshold, under a 5000 GtC perturbation, the boundary between safety and vulnerability is at $S_{\text{eff}} = 0.82$, e.g. 1.10 au from the star when orbiting a host identical to our Sun, with an initial pCO₂=4.6 x 10⁻⁴ bar (see black line segment in the bottom-left panel of Fig. 4). At 50,000 GtC, the boundary moves out to $S_{\text{eff}}=0.78$, or 1.13 au, with an initial pCO₂=4.5 x 10⁻³ bar (black line segment in the bottom-right panel of Fig. 4). The pH stability zones for 5000 GtC and 50,000 GtC both lie closer to the star than their temperature-stability analogues, so in the rest of the article, “stability zone” will refer to the more conservative temperature-based zones.

4. Discussion

4.1. Mechanisms of catastrophe & mass extinction

Hyperthermals and potentially one or more of the snowball events in Earth’s past were caused by transient carbon cycle perturbations, and these events strongly influenced the particular evolutionary path taken by the biosphere. Significant warming and/or ocean acidification, often as a result of the eruption of LIPs, is associated with most or all of the major mass extinctions in the Phanerozoic [Bond

& Grasby (2017), Lindström et al. (2017), Benton (2018), Racki et al. (2018), Schoene et al. (2019), Bond & Grasby (2020)]. The stability of global-mean surface temperature and ocean pH against transient carbon cycle perturbations on planets in the mid-to-outer reaches of the HZ suggests that such catastrophic climate events and mass extinctions may happen much less frequently for this class of Earth-like planet than they have on Earth. However, mass extinctions and climate perturbations can be caused by mechanisms other than temperature- and pH-change from CO₂ perturbations. It is worth examining the mechanisms underlying the catastrophes in Earth's past for context to understand the implications of the results in this paper.

A relevant category of catastrophic environmental processes is the set that can or must be triggered by an initial pulse of warming. Processes of this type have been important in past mass extinction events, and the resistance to CO₂-based temperature change on mid-outer HZ planets should make them less likely. Ocean anoxia is one such process. Ocean anoxia can be caused by increased continental weathering—a result of elevated temperature and/or pCO₂—which washes nutrients into the oceans and causes eutrophication, leading to elevated oxygen consumption that depletes surrounding waters [Bond & Grasby (2017)]. High surface temperatures can also directly cause anoxic events by productivity stimulation [Bond & Grasby (2017)] and enhanced ocean stratification (which reduces ocean ventilation) [Erbacher et al. (2001)]. However, productivity stimulation from the direct injection of nutrients into the ocean by seafloor LIP eruptions can also cause anoxia [Ernst & Youbi (2017)], so a lack of CO₂-based warming does not necessarily preclude anoxic conditions from occurring. Similarly, thermogenic methane release and consequent rapid warming can be caused by an initial pulse of CO₂ warming, but it can also be caused by the intrusion of LIP magmas into organic-rich sediments and coal beds [Bond & Grasby (2017)]. A final example of this type is the depletion of the ozone layer, which leads to elevated surface ultraviolet fluxes and is suggested to have contributed to several mass extinctions via UV's ability to induce harmful elevated mutation rates [Beerling et al. (2007), Bond & Grasby (2017), Marshall et al. (2020)]. [Marshall et al. (2020)] suggest that rapid warming may induce ozone loss via enhanced convective transport of ClO

into the stratosphere, but other mechanisms have also been proposed to destroy the ozone layer, such as supernova-accelerated cosmic ray bombardment [Fields et al. (2020)], organohalogen release by LIP volcanism [Beerling et al. (2007), Broadley et al. (2018)], or proton bombardment from flaring by an active M-dwarf star [Segura et al. (2010), Tilley et al. (2019)].

Along with increased resilience to hyperthermal-related disasters, these results suggest that planets in the mid-to-outer reaches of the HZ have reduced susceptibility to global glaciation from transient increases in weathering. Changes to lithology, continent location, mountain-building, and many other processes can all cause weathering to accelerate or decline (e.g. [Kump et al. (2000), Penman et al. (2020)]), and workers have suggested that several partial [Macdonald et al. (2019)] and global [Godd ris et al. (2003), Donnadi u et al. (2004), Cox et al. (2016)] glaciations happened as a result of weathering acceleration. Just like CO₂ injection leads to smaller temperature increases under high background pCO₂, CO₂ sequestration leads to smaller temperature reductions under the same conditions, meaning this route to glaciation may be much less likely for high pCO₂ planets. Still, if excess weathering can be maintained on long enough timescales, “limit cycling” (the alternation between a warm climate state and a snowball climate state due to lack of stable weathering equilibrium [Mills et al. (2011), Kadoya & Tajika (2014), Menou (2015), Abbot (2016), Haqq-Misra et al. (2016)]) remains a possibility for these planets, since the CO₂ drawdown events from which mid-outer HZ planets are safe are transient pulses, not the quasi-permanent shifts to new carbon cycle equilibria required for limit cycle initiation. In addition, other non-weathering-related mechanisms like a rapid reduction in the level of a non-CO₂ greenhouse gas like methane [Kopp et al. (2005)] or a rapid increase in albedo due to stratospheric aerosol injection [Macdonald & Wordsworth (2017)] have also been proposed to trigger glaciation [Arnscheidt & Rothman (2020)]. However, the high Rayleigh scattering albedo (see Fig. 2) and consequent reduced sensitivity of planetary albedo to surface albedo in high-pCO₂ atmospheres means the ice-albedo feedback is less effective on these planets, since the growth of sea ice has less effect on the radiative balance of the planet under high pCO₂ [Pierrehumbert (2010), Von Paris et al. (2013)]. A set of calculations (not shown) that included a

temperature-dependent surface albedo feedback using the formula in [Wang & Stone (1980)] yielded qualitatively identical behavior to the constant-surface-albedo calculations presented in this paper for both CO₂ increases and CO₂ decreases, confirming the basic result that climate stability increases with decreasing instellation.

There are also a variety of catastrophe-inducing mechanisms that are not triggered by carbon cycle perturbations or their downstream effects. The frequencies of these events should not be affected by the presence of high background pCO₂. For example, extraterrestrial disaster sources like nearby supernovae (which may have a variety of negative impacts on atmospheric chemistry, e.g. [Reid et al. (1978)]), large asteroid/comet impacts [Alvarez et al. (1980), Hull et al. (2020)], and stellar superflares [Lingam & Loeb (2017)] likely do not discriminate by background pCO₂ levels. Similarly, global heavy metal poisoning by LIP volcanism [Lindström et al. (2019)] should remain a possible killing mechanism regardless of background pCO₂, though it is an interesting question whether this process alone could trigger a mass extinction without the additional environmental stressors from an accompanying hyperthermal episode. A variety of catastrophe triggers remain in play for mid-outer HZ planets despite the results of this study, but the main mass extinction mechanisms that have operated in Earth's past may be suppressed on these planets.

A corollary to the reasoning that planets at lower luminosity than the Earth are more stable to CO₂ perturbation-induced extinctions is that planets in the HZ receiving more instellation than Earth will be more susceptible to these perturbations because of their lower initial pCO₂ (although it is worth noting that Earth's position near the inner edge of the HZ means that there is not much space for temperate planets to reside at higher instellations). This point is noted in a blog post by Alex Tolley, who suggests that the increased volatility might be a serious enough barrier to habitability to justify revising the inner edge of the HZ outward to a slightly greater distance from the star [Tolley (2018)]. The same basic idea is elaborated by [Archer (2016)], who shows that anthropogenic climate

change would be progressing even more rapidly if Earth had possessed a lower initial $p\text{CO}_2$ when industrialization began and less rapidly if the initial $p\text{CO}_2$ had been higher.

In line with the logic of [Archer (2016)] and analogous to the reasoning presented in the discussion of previous mass extinctions on Earth, the results in this paper also show that civilizations arising throughout a large proportion of the HZ would be placed in no danger of self-induced climate change by burning fossil fuels. Since 5000 GtC is an approximate upper-bound on the accessible fossil fuel inventory on Earth [Ramirez et al. (2014)], civilizations arising anywhere beyond the inner boundary of the 5000 GtC stability zone will not face the degree of CO_2 -based danger we face. Civilizational die-off from industrialization and pollution [Frank et al. (2018)] may be less of a danger on other worlds than it appears when extrapolating from Earth.

4.2. Does high $p\text{CO}_2$ preclude complex life?

A few studies have argued that high levels of atmospheric CO_2 may prevent the evolution of complex life on planets in the mid-outer reaches of the HZ [Bounama & Franck (2007), Schwieterman et al. (2019), Ramirez (2020)]. With the assumption of some threshold CO_2 beyond which complex life is not able to evolve, this idea can be used to define a “habitable zone for complex life” (HZCL), where temperatures can be maintained above freezing under the proposed CO_2 constraint. These arguments are based on observed responses of some forms of multicellular Earth-life, usually mammals, to high CO_2 , low pH, and/or high CO (which can build up to high levels in high- CO_2 atmospheres of planets orbiting cool M or K stars [Schwieterman et al. (2019)]). It is important to note that the idea that CO might limit complex life is falsified by the fact that some extant invertebrates are invulnerable to CO’s toxic effects because of their use of blood oxygen transport mechanisms that do not interact with CO [Howell (2019)]. Similarly, it is plausible that the pH- and $p\text{CO}_2$ -sensitivity of the organisms that have been studied are not results of fundamental constraints on complex life, but are instead results of the specific chemical machinery employed by particular

Earth lineages, a point which is acknowledged in the studies that explore the HZCL idea

[Schwieterman et al. (2019), Ramirez (2020)].

Still, if complex life is limited by high $p\text{CO}_2$, this has interesting implications for the results in this study. Using the most conservative value for maximum $p\text{CO}_2$ that appears in [Bounama & Franck (2007), Schwieterman et al. (2019), Ramirez (2020)], 0.01 bar, produces an outer edge for the HZCL of $S_{\text{eff}}=0.76$ with the climate model used in this paper, implying an outer radius of $d = 1.15$ au. This means there is no overlap between this conservative choice of HZCL and the 50,000 GtC stability zone defined in this paper (see Section 3.1), and only a narrow ring of overlap with the 5000 GtC stability zone ($1.15-1.12 = 0.03$ au). So, if the tolerance of complex life for CO_2 is low, this would suggest that much of the complex life in the universe could face carbon cycle volatility comparable to what the Earth experienced during the Phanerozoic Eon, conditional on significant similarities to Earth in terms of tectonics, mantle processes, and surface processes.

Alternatively, if we take the value for the outer edge of the HZCL to be at the luminosity where $p\text{CO}_2=0.1$ bar and $T=273.15$ K, perhaps based on the argument from lipid solubility theory in [Ramirez (2020)], the model used in this paper produces $S_{\text{eff}}=0.67$ and $d = 1.22$ au. With a 1D latitudinally-dependent energy balance climate model, [Ramirez (2020)] reports a slightly more distant boundary of $d = 1.27$ au with 1 bar background N_2 . Our preference is for the latter value, since it comes from a more sophisticated model, in which case the HZCL encompasses the entire 5000 GtC stability zone, as well as a small ring with a width of 0.07 au in the interior portion for the 50,000 GtC stability zone. Higher choices of the toxic $p\text{CO}_2$ level lead to greater overlap with the 50,000 GtC stability zone. So, under the less conservative choices for maximum $p\text{CO}_2$, there is an optimal zone that allows for CO_2 levels that are high enough to reduce climate sensitivity to carbon cycle perturbations while being small enough to allow complex life to flourish. Planets in this zone might be considered “superhabitable” [Heller & Armstrong (2014)].

4.3. Implications for distribution of biosignatures?

Corresponding Author: R.J. Graham, robert.graham@physics.ox.ac.uk

As mentioned in the introduction, the largest known extinction in Earth's history is the Permian-Triassic event, a crisis apparently triggered by the eruption of a LIP, which eliminated up to 96% of marine species (and a significant but potentially smaller fraction of species on land) [Bond & Wignall (2014), Benton (2018)]. Several other mass extinctions that eliminated most of the species on Earth at the time also coincided with LIP eruptions [Kidder & Worsley (2010), Bond & Grasby (2017)]. The severity and frequency of these mass extinctions in Earth history raises the question of whether they present a danger to the persistence of complex biospheres over geologic timescales – it is conceivable that the Permian-Triassic extinction might have wiped out 100% of macroscopic species had the event been somewhat more severe.

If large, productive oxygenic biospheres are difficult to maintain for long periods because of extinction events, planets with detectable O_2/O_3 biosignatures may be few and far between, and thus difficult to find with near-future telescope surveys (see e.g. [Kawashima & Rugheimer (2019), Checlair et al. (2020)] for discussions of next-generation O_2/O_3 biosignature detection). In a work addressing the question of the persistence of Earth-like biospheres in the face of extinction events, [Tsumura (2020)] models Earth's extinction history as a random multiplicative process, and his methodology leads him to conclude that the probability of life's survival on Earth from the time of its origin to the present day is only 15% (since it is likely extremely difficult to extinguish prokaryotic life, this result should appropriately be considered to apply only to complex, multicellular life, not life as a whole). [Tsumura (2020)] suggests that this value can be used in models attempting to estimate the prevalence of intelligent life in the universe.

The results in this article demonstrate that Tsumura's calculations cannot be applied to infer the rate of complex life sterilization on Earth-like planets in general, even if they do accurately represent Earth itself. This is because the mechanisms that produced Earth's particular extinction history are strongly dependent on background atmospheric state, which is expected to systematically vary. In particular, the increased resilience to carbon cycle perturbations of planets in the mid-outer HZ

implies that these planets will be much less susceptible to the primary form of mass extinction that has operated on Earth, suggesting a higher long-term survival fraction for complex biospheres that occupy the stability zones outlined in Section 3.

Overall, this discussion implies that O_2/O_3 biosignatures may be more common in the middle-outer reaches of the HZ compared to the innermost region due to reduced likelihood of extinction because of greater environmental stability under high- pCO_2 atmospheres. For planets orbiting F-, G- and early-K-type stars that display significant brightening on gigayear timescales, this might suggest an anti-correlation between stellar age and biosignature prevalence because the increase in luminosity pushes the location of stability zones farther and farther away from the star over time, moving a larger and larger fraction of planets into the less-stable, more-extinction-prone interior region of the HZ. This prediction is directly opposite that of [Bixel & Apai (2020)], who note that the appearance of detectable O_2/O_3 biosignatures on Earth occurred one to two billion years after the origin of life, suggesting that planets orbiting older stars may be better candidates for biosignature searches.

An identical point regarding safety from catastrophic sterilization can be made about the distribution of technosignatures (biosignatures that imply the presence of technological civilizations e.g. [Lin et al. (2014)]). As noted in Section 4.1, analogues of anthropogenic climate change will be much less severe on planets in the stability zones defined in this paper, which suggests that civilizations on these planets may experience less stress from industrialization than those at higher instellations, perhaps allowing them to persist longer and increasing the likelihood of observable technosignatures in the stability zones.

Another wrinkle in this discussion is the possibility that non-sterilizing mass extinctions and climatic perturbations facilitate the emergence of novelty in the biosphere by freeing up or creating niches and restructuring ecosystems, perhaps allowing for greater complexity/biodiversity to be attained post-recovery e.g. [Wagner et al. (2006)]. An extreme example of this is the suggestion that

the Neoproterozoic snowball Earth episodes triggered the emergence of animal multicellularity [Simpson (2019)]. If climate perturbations do have a long-term positive effect on global biodiversity and novelty, then it is possible that planets in the stability zones will be less likely to have detectable biosignatures, depending on whether this effect is more important than the possibility of sterilization of complex life. However, the ecological and biogeochemical dynamics of post-catastrophe recovery are complex and poorly understood [Solé et al. (2002), Hull (2015)], and the paleontological data on the long-term impact of non-sterilizing catastrophes on global biodiversity is open to various interpretations [Michael Foote, personal communication].

So, biosignatures may be more likely in the high $p\text{CO}_2$ stability zones. This selection criterion can be used in conjunction with others, e.g. the HZCL [Schwieterman et al. (2019), Ramirez (2020)], to rank and prioritize targets in the HZ for next-generation telescopes to probe in search of life. If decreased likelihood of catastrophe leads to a greater likelihood of detectable biosignatures, a large enough sample of O_2/O_3 detections might reveal a trend with a higher-than-expected fraction of biosignature detections at low instellations within the HZ.

4.4. Implications for Earth history?

Although there is still considerable debate about Earth's CO_2 levels throughout the past 4 Ga (e.g. [Charnay et al. (2020)]), recent proxy constraints suggest that CO_2 partial pressure may have been approximately 1000x its present value (perhaps $\sim 0.1\text{-}0.5$ bar) in the late Archean [Lehmer et al. (2020), Payne et al. (2020)], with a gradual decline over the Proterozoic Eon driven by the response of weathering to a brightening Sun [Kanzaki & Murakami (2015), Krissansen-Totton et al. (2018), Krissansen-Totton & Catling (2020)]. The role of other greenhouse gases during the Precambrian is unclear, but there is some evidence for strongly elevated methane levels during the Archean, which may also have accounted for some of the warming needed to offset the climate impacts of the dimmer young Sun [Catling & Zahnle (2020)]. Probabilistic models of ocean pH through geologic time that account for the wide uncertainties in relevant proxy data produce a corresponding history with

pH increasing from an initial slightly acidic-to-neutral range of 6.5-7 in the Archean to a slightly basic range of 7.5 to 9 during the Phanerozoic [Halevy & Bachan (2017), Krissansen-Totton et al. (2018), Krissansen-Totton & Catling (2020)].

High values of $p\text{CO}_2$ and low values of ocean pH in Earth's past would suggest that the planet may have exhibited the stability to CO_2 perturbations described in this paper during the Archean and part of the Proterozoic. Much of the Precambrian seems to have displayed notable climatic stability and warmth, particularly after the major period of global glaciation leading from the Archean into the Proterozoic, which may have marked the transition from an oxygen-poor atmosphere with strong greenhouse warming from both CO_2 and CH_4 to an oxidized atmosphere with limited CH_4 warming [Daines & Lenton (2016), Olson et al. (2016), Catling & Zahnle (2020)]. With $p\text{CO}_2$ held at high levels (perhaps 0.01-0.1 bar) by the silicate weathering feedback [Krissansen-Totton et al. (2018)] and, potentially, CO_2 -generating authigenic clay formation ("reverse weathering") [Isson & Planavsky (2018), Krissansen-Totton & Catling (2020)], the mid-Proterozoic atmosphere would have been quite stable to transient CO_2 release and/or consumption from the many LIPs recorded during this period [Ernst & Youbi (2017)]. This may partially explain the apparent lack of transient climate extremes during the "Boring Billion" period [Buick et al. (1995)] between approximately 1.7 to 0.75 Ga, though underlying geologic causes are still necessary to explain the long-lasting warm, steady background climate [Cawood & Hawkesworth (2014)]. The stability to CO_2 perturbations would have decreased over time as increasing solar luminosity caused CO_2 to be drawn down, which may have been a necessary precondition that allowed for transient enhanced weathering events to trigger one or both of the Neoproterozoic snowball episodes [Godd ris et al. (2003), Donnadieu et al. (2004)]. Even in the Phanerozoic, the issue of background $p\text{CO}_2$ and its influence on the sensitivity of climate to a given increase/decrease in CO_2 plays an important role in the debate over the interpretation of the evidence for events like the Paleocene-Eocene Thermal Maximum [Pagani et al. (2006), Higgins & Schrag (2006)].

Corresponding Author: R.J. Graham, robert.graham@physics.ox.ac.uk

The remaining lifespan of the complex biosphere is estimated to be ~ 1 Ga based on the modeled timing of the drawdown of atmospheric CO_2 to a level below the lower limits of tolerance for C4 plants as the Sun continues to brighten [Caldeira & Kasting (1992)]. However, a severe LIP eruption could conceivably end complex life much earlier, similar to the suggestion that a LIP eruption ended habitable conditions on Venus [Ernst et al. (2017), Way & Del Genio (2020)]. The low CO_2 conditions of Earth's future should make environmental conditions even more sensitive to CO_2 perturbations than they were during past LIPs. However, the evolution of pelagic calcifiers over the past 200 million years may have strongly increased environmental resilience to CO_2 perturbations [Henehan et al. (2016)], suggesting a potential counter to the effects of reduced CO_2 . A biogeochemical model that includes the effects of pelagic calcifiers on ocean chemistry could be used to examine the impact of future LIP eruptions under low $p\text{CO}_2$, high insolation conditions.

5. Summary & Conclusions

In this article, we used idealized climate and ocean chemistry models to demonstrate that high $p\text{CO}_2$ atmospheres on planets in the middle and outer regions of the HZ confer robust temperature- and pH-stability in the face of CO_2 perturbations that would cause severe environmental change in the low- $p\text{CO}_2$ context of Phanerozoic Earth. Both temperature- and pH-stability arise because of the rapid growth in $p\text{CO}_2$ necessary to maintain a temperate climate as instellation decreases with distance from the host star on planets with $\text{N}_2\text{-CO}_2\text{-H}_2\text{O}$ atmospheres in the HZ. The $p\text{CO}_2$ necessary for above-freezing temperatures at the outer edge of the HZ can be more than a million times greater than that required near the inner edge, assuming constant $p\text{N}_2$, so CO_2 's logarithmic radiative forcing response means that a given mass of CO_2 added to or subtracted from the atmosphere of a temperate planet near the inner edge has a vastly larger effect on surface temperature than the same change in atmospheric CO_2 mass near the outer edge. Similarly, as $p\text{CO}_2$ increases, there is a reduction in the fraction of CO_2 that partitions into the ocean as dissolved inorganic carbon for a given

mass of carbon injected into the atmosphere-ocean system, meaning the marginal impact of a given CO₂ change on ocean pH decreases as background levels go up.

The CO₂ perturbations imposed in the experiments in this study are equivalent to 5000 GtC and 50,000 GtC added to the atmosphere, which are, respectively, an estimate of the amount of carbon that would be released if all accessible fossil fuels were burnt [Ramirez et al. (2014)] and a high estimate of the amount of carbon released due to LIP volcanism during the most severe mass extinction in Earth history [Kump (2018)]. The temperature response to the 5000 GtC perturbation falls below 4 K at $S_{\text{eff}}=0.8$, where the initial $p\text{CO}_2=1.5 \times 10^{-3}$ bar, corresponding to an orbital distance of $d = 1.12$ au in the Solar System. The temperature response to the 50,000 GtC perturbation reaches the same 4 K threshold at $S_{\text{eff}}=0.7$ and $p\text{CO}_2=5.4 \times 10^{-2}$ bar, corresponding to $d=1.2$ au. Those values of d can serve as inner boundaries for “stability zones” where N₂-CO₂-H₂O atmospheres are relatively invulnerable to temperature effects of CO₂ changes at or below a given magnitude (see Fig. 5). Analogously, the magnitude of pH reduction falls below 0.5 units at $S_{\text{eff}}=0.82$ ($d=1.1$ au) and $S_{\text{eff}}=0.78$ ($d=1.13$ au) for 5000 GtC and 50,000 GtC perturbations respectively.

These results suggest that many Earth-like planets throughout the mid-to-outer habitable zone may be safe from extreme environmental change from transient CO₂ perturbations of sizes that have caused catastrophes in Earth’s past, particularly planets in the 50,000 GtC stability zone (Figs. 4, 5). Similarly, climate change and ocean acidification from CO₂ emitted by the burning of fossil fuels may be a less serious issue for civilizations on planets receiving less instellation than Earth (see 5000 GtC stability zone in Fig. 5). This represents a significant habitability advantage for temperate planets in the mid-to-outer reaches of the HZ compared to those near the inner edge. The large climate swings that have punctuated the Phanerozoic Eon are in part a result of Earth’s low $p\text{CO}_2$ and relative proximity to the inner edge of the habitable zone during this period.

Acknowledgments

I thank Ray Pierrehumbert, Dorian Abbot, Michael Foote, and Sarah Rugheimer for useful discussions over the

course of the writing of this paper. I also thank Ray, Dorian, Sarah, and two anonymous reviewers for helpful comments on various versions of the manuscript.

Disclosure statement

I have no conflicts of interest.

Funding

I gratefully acknowledge scholarship funding from the Clarendon Fund and Jesus College, Oxford.

[Abbot (2016)] Abbot, D. S. (2016), 'Analytical investigation of the decrease in the size of the habitable zone due to limited CO₂ outgassing rate', *The Astrophysical Journal* **827**, 117.

[Alvarez et al. (1980)] Alvarez, L. W., Alvarez, W., Asaro, F. & Michel, H. V. (1980), 'Extraterrestrial cause for the Cretaceous-Tertiary extinction', *Science* **208**(4448), 1095–1108.

[Archer (2016)] Archer, D. (2016), 'Near miss: the importance of the natural atmospheric CO₂ concentration to human historical evolution', *Climatic Change* **138**(1-2), 1–11.

[Arnscheidt & Rothman (2020)] Arnscheidt, C. W. & Rothman, D. H. (2020), 'Routes to global glaciation', *Proceedings of the Royal Society A* **476**(2239), 20200303.

[Bean et al. (2017)] Bean, J. L., Abbot, D. S. & Kempton, E. M.-R. (2017), 'A statistical comparative planetology approach to the hunt for habitable exoplanets and life beyond the solar system', *The Astrophysical Journal* **841**, L24.

[Beerling et al. (2007)] Beerling, D. J., Harfoot, M., Lomax, B. & Pyle, J. A. (2007), 'The stability of the stratospheric ozone layer during the end-Permian eruption of the Siberian traps', *Philosophical Transactions of the Royal Society A: Mathematical, Physical and Engineering Sciences* **365**(1856), 1843–1866.

[Benton (2018)] Benton, M. J. (2018), 'Hyperthermal-driven mass extinctions: killing models during the Permian-Triassic mass extinction', *Philosophical Transactions of the Royal Society A: Mathematical, Physical and Engineering Sciences* **376**(2130), 20170076.

[Bixel & Apai (2020)] Bixel, A. & Apai, D. (2020), 'Testing earthlike atmospheric evolution on exo-Earths through oxygen absorption: Required sample sizes and the advantage of age-based target selection', *The Astrophysical Journal* **896**(2), 131. <http://dx.doi.org/10.3847/1538-4357/ab8fad>

[Bond & Grasby (2017)] Bond, D. P. & Grasby, S. E. (2017), 'On the causes of mass extinctions', *Palaeogeography, Palaeoclimatology, Palaeoecology* **478**, 3–29.

[Bond & Grasby (2020)] Bond, D. P. & Grasby, S. E. (2020), 'Late Ordovician mass extinction caused by volcanism, warming, and anoxia, not cooling and glaciation', *Geology*.

[Bond & Wignall (2014)] Bond, D. P. & Wignall, P. B. (2014), 'Large igneous provinces and mass extinctions: an update', *Volcanism, impacts, and mass extinctions: causes and effects* **505**, 29–55.

[Bounama & Franck (2007)] Bounama, C., W. v. B. & Franck, S. (2007), 'How rare is complex life in the Milky Way?', *Astrobiology*.

- [Broadley et al. (2018)] Broadley, M. W., Barry, P. H., Ballentine, C. J., Taylor, L. A. & Burgess, R. (2018), 'End-permian extinction amplified by plume-induced release of recycled lithospheric volatiles', *Nature Geoscience* **11**(9), 682.
- [Buick et al. (1995)] Buick, R., Des Marais, D. J. & Knoll, A. H. (1995), 'Stable isotopic compositions of carbonates from the mesoproterozoic bangemall group, northwestern australia', *Chemical Geology* **123**(1-4), 153–171.
- [Caldeira & Kasting (1992)] Caldeira, K. & Kasting, J. (1992), 'The life-span of the biosphere revisited', *Nature* **360**(6406), 721–723.
- [Catling & Zahnle (2020)] Catling, D. C. & Zahnle, K. J. (2020), 'The archean atmosphere', *Science Advances* **6**(9), eaax1420.
- [Cawood & Hawkesworth (2014)] Cawood, P. A. & Hawkesworth, C. J. (2014), 'Earth's middle age', *Geology* **42**(6), 503–506.
- [Charnay et al. (2020)] Charnay, B., Wolf, E. T., Marty, B. & Forget, F. (2020), 'Is the faint young sun problem for earth solved?', *arXiv preprint arXiv:2006.06265* .
- [Checlair et al. (2020)] Checlair, J. H., Hayworth, B. P., Olson, S. L., Komacek, T. D., Villanueva, G. L., Popovic, P., Yang, H. & Abbot, D. S. (2020), 'Non-detection of O_2/O_3 informs frequency of earth-like planets with luvoir but not habex', *arXiv preprint arXiv:2008.03952* .
- [Colbourn et al. (2015)] Colbourn, G., Ridgwell, A. & Lenton, T. (2015), 'The time scale of the silicate weathering negative feedback on atmospheric CO_2 ', *Global Biogeochemical Cycles* **29**(5), 583–596.
- [Coogan & Gillis (2013)] Coogan, L. A. & Gillis, K. M. (2013), 'Evidence that low-temperature oceanic hydrothermal systems play an important role in the silicate-carbonate weathering cycle and long-term climate regulation', *Geochemistry, Geophysics, Geosystems* **14**(6), 1771–1786.
- [Cox et al. (2016)] Cox, G. M., Halverson, G. P., Stevenson, R. K., Vokaty, M., Poirier, A., Kunzmann, M., Li, Z.-X., Denyszyn, S. W., Strauss, J. V. & Macdonald, F. A. (2016), 'Continental flood basalt weathering as a trigger for neoproterozoic snowball earth', *Earth and Planetary Science Letters* **446**, 89–99.
- [Cronin (2014)] Cronin, T. W. (2014), 'On the choice of average solar zenith angle', *Journal of the Atmospheric Sciences* **71**(8), 2994–3003.
- [Daines & Lenton (2016)] Daines, S. J. & Lenton, T. M. (2016), 'The effect of widespread early aerobic marine ecosystems on methane cycling and the great oxidation', *Earth and Planetary Science Letters* **434**, 42–51.
- [Donnadieu et al. (2004)] Donnadieu, Y., Godderis, Y., Ramstein, G., Nedelec, A. & Meert, J. (2004), 'A 'Snowball Earth' climate triggered by continental break-up through changes in runoff', *Nature* **428**(6980), 303–306.
- [Erbacher et al. (2001)] Erbacher, J., Huber, B. T., Norris, R. D. & Markey, M. (2001), 'Increased thermohaline stratification as a possible cause for an ocean anoxic event in the cretaceous period', *Nature* **409**(6818), 325–327.
- [Ernst et al. (2017)] Ernst, R. E., Buchan, K. L., Jowitt, S. M. & Youbi, N. (2017), 'Applying the terrestrial large igneous provinces (lips) context to large-scale magmatism on other planetary bodies'.
- [Ernst & Youbi (2017)] Ernst, R. E. & Youbi, N. (2017), 'How large igneous provinces affect global climate, sometimes cause mass extinctions, and represent natural markers in the geological record', *Palaeogeography, palaeoclimatology, palaeoecology* **478**, 30–52.

- [Fields et al. (2020)] Fields, B. D., Melott, A. L., Ellis, J., Ertel, A. F., Fry, B. J., Lieberman, B. S., Liu, Z., Miller, J. A. & Thomas, B. C. (2020), 'Supernova triggers for end-devonian extinctions', *Proceedings of the National Academy of Sciences* .
- [Foster et al. (2018)] Foster, G. L., Hull, P., Lunt, D. J. & Zachos, J. C. (2018), 'Placing our current "hyperthermal" in the context of rapid climate change in our geological past'.
- [Frank et al. (2018)] Frank, A., Carroll-Nellenback, J., Alberti, M. & Kleidon, A. (2018), 'The anthropocene generalized: evolution of exo-civilizations and their planetary feedback', *Astrobiology* **18**(5), 503–518.
- [Godd ris et al. (2003)] Godd ris, Y., Donnadi u, Y., N d lec, A., Dupr , B., Dessert, C., Grard, A., Ramstein, G. & Fran ois, L. (2003), 'The sturtian "snowball" glaciation: fire and ice', *Earth and planetary science letters* **211**(1-2), 1–12.
- [Goldblatt et al. (2021)] Goldblatt, C., McDonald, V. L. & McCusker, K. E. (2021), 'Earth's long-term climate stabilized by clouds', *Nature Geoscience* pp. 1–8.
- [Goldblatt & Watson (2012)] Goldblatt, C. & Watson, A. J. (2012), 'The runaway greenhouse: implications for future climate change, geoengineering and planetary atmospheres', *Philosophical Transactions Of The Royal Society A-Mathematical Physical And Engineering Sciences* **370**(1974), 4197–4216.
- [Graham & Pierrehumbert (2020)] Graham, R. & Pierrehumbert, R. (2020), 'Thermodynamic and energetic limits on continental silicate weathering strongly impact the climate and habitability of wet, rocky worlds', *Astrophysical Journal* **896**(2).
- [Halevy & Bachan (2017)] Halevy, I. & Bachan, A. (2017), 'The geologic history of seawater ph', *Science* **355**(6329), 1069–1071.
- [Haqq-Misra et al. (2016)] Haqq-Misra, J., Kopparapu, R. K., Batalha, N. E., Harman, C. E. & Kasting, J. F. (2016), 'Limit cycles can reduce the width of the habitable zone', *The Astrophysical Journal* **827**(2), 120.
- [Heller & Armstrong (2014)] Heller, R. & Armstrong, J. (2014), 'Superhabitable worlds', *Astrobiology* **14**(1), 50–66.
- [Henehan et al. (2016)] Henehan, M. J., Hull, P. M., Penman, D. E., Rae, J. W. & Schmidt, D. N. (2016), 'Biogeochemical significance of pelagic ecosystem function: an end-cretaceous case study', *Philosophical Transactions of the Royal Society B: Biological Sciences* **371**(1694), 20150510.
- [Higgins & Schrag (2006)] Higgins, J. A. & Schrag, D. P. (2006), 'Beyond methane: Towards a theory for the Paleocene-Eocene Thermal Maximum', *Earth and Planetary Science Letters* **245**(3-4), 523–537. DOI: 10.1016/j.epsl.2006.03.009.
- [Howell (2019)] Howell, J. E. (2019), 'Comment on " a limited habitable zone for complex life" (schwartzman et al. 2019 apj 878, 19)', *Research Notes of the AAS* **3**(6), 85.
- [Huang & Bani Shahabadi (2014)] Huang, Y. & Bani Shahabadi, M. (2014), 'Why logarithmic? a note on the dependence of radiative forcing on gas concentration', *Journal of Geophysical Research: Atmospheres* **119**(24), 13–683.
- [Hull (2015)] Hull, P. (2015), 'Life in the aftermath of mass extinctions', *Current Biology* **25**(19), R941–R952.
- [Hull et al. (2020)] Hull, P. M., Bornemann, A., Penman, D. E., Henehan, M. J., Norris, R. D., Wilson, P. A., Blum, P., Alegret, L., Batenburg, S. J., Bown, P. R. et al. (2020), 'On impact and volcanism across the cretaceous-paleogene boundary', *science* **367**(6475), 266–272.

- [Ingersoll (1969)] Ingersoll, A. (1969), 'The runaway greenhouse: A history of water on venus', *J. Atmos. Sci.* **26**, 1191–1198.
- [Isson & Planavsky (2018)] Isson, T. T. & Planavsky, N. J. (2018), 'Reverse weathering as a long-term stabilizer of marine pH and planetary climate', *Nature* **560**(7719), 471.
- [Jacobson (2005)] Jacobson, M. Z. (2005), 'Studying ocean acidification with conservative, stable numerical schemes for nonequilibrium air-ocean exchange and ocean equilibrium chemistry', *Journal of Geophysical Research: Atmospheres* **110**(D7).
- [Kadoya & Tajika (2014)] Kadoya, S. & Tajika, E. (2014), 'Conditions for oceans on earth-like planets orbiting within the habitable zone: Importance of volcanic CO₂ degassing', *The Astrophysical Journal* **790**(2), 107.
- [Kadoya & Tajika (2019)] Kadoya, S. & Tajika, E. (2019), 'Outer limits of the habitable zones in terms of climate mode and climate evolution of earth-like planets', *The Astrophysical Journal* **875**(1), 7.
- [Kanzaki & Murakami (2015)] Kanzaki, Y. & Murakami, T. (2015), 'Estimates of atmospheric CO₂ in the neoproterozoic–paleoproterozoic from paleosols', *Geochimica et Cosmochimica Acta* **159**, 190–219.
- [Kasting (1991)] Kasting, J. F. (1991), 'CO₂ condensation and the climate of early Mars', *Icarus* **94**(1), 1–13.
- [Kasting et al. (1984)] Kasting, J. F., Pollack, J. B. & Ackerman, T. P. (1984), 'Response of Earth's atmosphere to increases in solar flux and implications for loss of water from Venus', *Icarus* **57**(3), 335–355.
- [Kasting et al. (1988)] Kasting, J. F., Toon, O. B. & Pollack, J. B. (1988), 'How climate evolved on the terrestrial planets', *Scientific American* **258**(2), 90–97.
- [Kasting et al. (1993)] Kasting, J. F., Whitmire, D. P. & Reynolds, R. T. (1993), 'Habitable zones around main-sequence stars', *Icarus* **101**(1), 108–128.
- [Kawashima & Rugheimer (2019)] Kawashima, Y. & Rugheimer, S. (2019), 'Theoretical reflectance spectra of earth-like planets through their evolutions: Impact of clouds on the detectability of oxygen, water, and methane with future direct imaging missions', *The Astronomical Journal* **157**(5), 213.
- [Kidder & Worsley (2010)] Kidder, D. L. & Worsley, T. R. (2010), 'Phanerozoic large igneous provinces (LIPs), heat (haline euxinic acidic thermal transgression) episodes, and mass extinctions', *Palaeogeography, Palaeoclimatology, Palaeoecology* **295**(1-2), 162–191.
- [Kopp et al. (2005)] Kopp, R., Kirschvink, J., Hilburn, I. & Nash, C. (2005), 'The paleoproterozoic snowball earth: A climate disaster triggered by the evolution of oxygenic photosynthesis', *PNAS* **102**(32), 11131–11136. doi:10.1073/pnas.0504878102.
- [Kopparapu et al. (2013)] Kopparapu, R. K., Ramirez, R., Kasting, J. F., Eymet, V., Robinson, T. D., Mahadevan, S., Terrien, R. C., Domagal-Goldman, S., Meadows, V. & Deshpande, R. (2013), 'Habitable Zones around Main-sequence Stars: New Estimates', *The Astrophysical Journal* **765**(2), 131.
- [Krissansen-Totton et al. (2018)] Krissansen-Totton, J., Arney, G. N. & Catling, D. C. (2018), 'Constraining the climate and ocean pH of the early earth with a geological carbon cycle model', *Proceedings of the National Academy of Sciences* **115**(16), 4105–4110.
- [Krissansen-Totton & Catling (2020)] Krissansen-Totton, J. & Catling, D. C. (2020), 'A coupled carbon-silicon cycle model over earth history: Reverse weathering as a possible explanation of a warm mid-proterozoic climate', *Earth and Planetary Science Letters* **537**, 116181.

- [Kump (2018)] Kump, L. R. (2018), 'Prolonged late permian–early triassic hyperthermal: failure of climate regulation?', *Philosophical Transactions of the Royal Society A: Mathematical, Physical and Engineering Sciences* **376**(2130), 20170078.
- [Kump et al. (2000)] Kump, L. R., Brantley, S. L. & Arthur, M. A. (2000), 'Chemical weathering, atmospheric co₂, and climate', *Annual Review of Earth and Planetary Sciences* **28**(1), 611–667.
- [Leconte et al. (2013)] Leconte, J., Forget, F., Charnay, B., Wordsworth, R. & Pottier, A. (2013), 'Increased insolation threshold for runaway greenhouse processes on Earth-like planets', *Nature* **504**(7479), 268–271.
- [Lehmer et al. (2020)] Lehmer, O., Catling, D., Buick, R., Brownlee, D. & Newport, S. (2020), 'Atmospheric co₂ levels from 2.7 billion years ago inferred from micrometeorite oxidation', *Science advances* **6**(4), eaay4644.
- [Lin et al. (2014)] Lin, H. W., Abad, G. G. & Loeb, A. (2014), 'Detecting industrial pollution in the atmospheres of earth-like exoplanets', *The Astrophysical Journal Letters* **792**(1), L7.
- [Lindström et al. (2019)] Lindström, S., Sanei, H., Van De Schootbrugge, B., Pedersen, G. K., Leshner, C. E., Tegner, C., Heunisch, C., Dybkjær, K. & Outridge, P. M. (2019), 'Volcanic mercury and mutagenesis in land plants during the end-triassic mass extinction', *Science advances* **5**(10), eaaw4018.
- [Lindström et al. (2017)] Lindström, S., van de Schootbrugge, B., Hansen, K. H., Pedersen, G. K., Alsen, P., Thibault, N., Dybkjær, K., Bjerrum, C. J. & Nielsen, L. H. (2017), 'A new correlation of triassic–jurassic boundary successions in nw europe, nevada and peru, and the central atlantic magmatic province: A time-line for the end-triassic mass extinction', *Palaeogeography, Palaeoclimatology, Palaeoecology* **478**, 80–102.
- [Lingam & Loeb (2017)] Lingam, M. & Loeb, A. (2017), 'Risks for life on habitable planets from superflares of their host stars', *The Astrophysical Journal* **848**(1), 41.
- [Macdonald et al. (2019)] Macdonald, F. A., Swanson-Hysell, N. L., Park, Y., Lisiecki, L. & Jagoutz, O. (2019), 'Arc-continent collisions in the tropics set earth's climate state', *Science* **364**(6436), 181–184.
- [Macdonald & Wordsworth (2017)] Macdonald, F. A. & Wordsworth, R. (2017), 'Initiation of snowball earth with volcanic sulfur aerosol emissions', *Geophysical Research Letters* **44**(4), 1938–1946.
- [Maher & Chamberlain (2014)] Maher, K. & Chamberlain, C. (2014), 'Hydrologic regulation of chemical weathering and the geologic carbon cycle', *science* **343**(6178), 1502–1504.
- [Marshall et al. (2020)] Marshall, J. E., Lakin, J., Troth, I. & Wallace-Johnson, S. M. (2020), 'Uv-b radiation was the devonian-carboniferous boundary terrestrial extinction kill mechanism', *Science Advances* **6**(22), eaba0768.
- [McInerney & Wing (2011)] McInerney, F. A. & Wing, S. L. (2011), 'The paleocene-eocene thermal maximum: a perturbation of carbon cycle, climate, and biosphere with implications for the future', *Annual Review of Earth and Planetary Sciences* **39**, 489–516.
- [Menou (2015)] Menou, K. (2015), 'Climate stability of habitable Earth-like planets', *Earth and Planetary Science Letters* **429**, 20–25.
- [Mills et al. (2011)] Mills, B., Watson, A. J., Goldblatt, C., Boyle, R. & Lenton, T. M. (2011), 'Timing of Neoproterozoic glaciations linked to transport-limited global weathering', *Nature Geosciences* **4**, 861–864. DOI: 10.1038/NGEO1305.

- [New et al. (2011)] New, M., Liverman, D., Schroder, H. & Anderson, K. (2011), 'Four degrees and beyond: the potential for a global temperature increase of four degrees and its implications', *Philosophical Transactions of the Royal Society A* **369**, 6–19.
- [Olson et al. (2016)] Olson, S. L., Reinhard, C. T. & Lyons, T. W. (2016), 'Limited role for methane in the mid-proterozoic greenhouse', *Proceedings of the National Academy of Sciences* **113**(41), 11447–11452.
- [Pagani et al. (2006)] Pagani, M., Caldeira, K., Archer, D. & Zachos, J. C. (2006), 'An ancient carbon mystery', *Science* **314**(5805), 1556–1557. DOI: 10.1126/science.1136110.
- [Payne et al. (2020)] Payne, R. C., Brownlee, D. & Kasting, J. F. (2020), 'Oxidized micrometeorites suggest either high pco₂ or low pn₂ during the neoproterozoic', *Proceedings of the National Academy of Sciences* **117**(3), 1360–1366.
- [Penman et al. (2020)] Penman, D. E., Rugenstein, J. K. C., Ibarra, D. E. & Winnick, M. J. (2020), 'Silicate weathering as a feedback and forcing in earth's climate and carbon cycle', *Earth-Science Reviews* p. 103298.
- [Pierrehumbert (1995)] Pierrehumbert, R. T. (1995), 'Thermostats, radiator fins, and the local runaway greenhouse', *Journal of the Atmospheric Sciences* **52**(10), 1784–1806.
- [Pierrehumbert (2010)] Pierrehumbert, R. T. (2010), *Principles of Planetary Climate*, Cambridge University Press.
- [Popp et al. (2016)] Popp, M., Schmidt, H. & Marotzke, J. (2016), 'Transition to a moist greenhouse with CO₂ and solar forcing', *Nature Communications* **7**, 10627.
- [Racki et al. (2018)] Racki, G., Rakocinski, M., Marynowski, L. & Wignall, P. B. (2018), 'Mercury enrichments and the frasnian-famennian biotic crisis: A volcanic trigger proved?', *Geology* **46**(6), 543–546.
- [Ramirez (2020)] Ramirez, R. M. (2020), 'A complex life habitable zone based on lipid solubility theory', *Scientific Reports* **10**(1), 1–8.
- [Ramirez et al. (2014)] Ramirez, R. M., Kopparapu, R. K., Lindner, V. & Kasting, J. F. (2014), 'Can increased atmospheric co₂ levels trigger a runaway greenhouse?', *Astrobiology* **14**(8), 714–731.
- [Reid et al. (1978)] Reid, G., McAfee, J. & Crutzen, P. (1978), 'Effects of intense stratospheric ionisation events', *Nature* **275**(5680), 489–492.
- [Rogner (1997)] Rogner, H.-H. (1997), 'An assessment of world hydrocarbon resources', *Annual review of energy and the environment* **22**(1), 217–262.
- [Rothman (2017)] Rothman, D. H. (2017), 'Thresholds of catastrophe in the earth system', *Science Advances* **3**(9), e1700906.
- [Sagan & Mullen (1972)] Sagan, C. & Mullen, G. (1972), 'Earth and mars - evolution of atmospheres and surface temperatures', *Science* **177**(4043), 52–56.
- [Schneider et al. (2019)] Schneider, T., Kaul, C. M. & Pressel, K. G. (2019), 'Possible climate transitions from breakup of stratocumulus decks under greenhouse warming', *Nature Geoscience* **12**(3), 163–167.
- [Schoene et al. (2019)] Schoene, B., Eddy, M. P., Samperton, K. M., Keller, C. B., Keller, G., Adatte, T. & Khadri, S. F. (2019), 'U-pb constraints on pulsed eruption of the deccan traps across the end-cretaceous mass extinction', *Science* **363**(6429), 862–866.

- [Schwieterman et al. (2019)] Schwieterman, E. W., Reinhard, C. T., Olson, S. L., Harman, C. E. & Lyons, T. W. (2019), 'A limited habitable zone for complex life', *The Astrophysical Journal* **878**(1), 19.
- [Seeley & Jeevanjee (2020)] Seeley, J. & Jeevanjee, N. (2020), 'H₂O windows and CO₂ radiator fins: a clear-sky explanation for the peak in ECS',
- [Segura et al. (2010)] Segura, A., Walkowicz, L. M., Meadows, V., Kasting, J. & Hawley, S. (2010), 'The effect of a strong stellar flare on the atmospheric chemistry of an earth-like planet orbiting an M dwarf', *Astrobiology* **10**(7), 751–771.
- [Simpson (2019)] Simpson, C. (2019), 'Complex multicellularity as an evolutionary response to viscous snowball earth oceans', *AGUFM* **2019**, PP54A–01.
- [Sobolev et al. (2011)] Sobolev, S. V., Sobolev, A. V., Kuzmin, D. V., Krivolutsкая, N. A., Petrunin, A. G., Arndt, N. T., Radko, V. A. & Vasiliev, Y. R. (2011), 'Linking mantle plumes, large igneous provinces and environmental catastrophes', *Nature* **477**(7364), 312–316.
- [Solé et al. (2002)] Solé, R. V., Montoya, J. M. & Erwin, D. H. (2002), 'Recovery after mass extinction: Evolutionary assembly in large-scale biosphere dynamics', *Philosophical Transactions of the Royal Society of London. Series B: Biological Sciences* **357**(1421), 697–707.
- [Somelar et al. (2020)] Somelar, P., Soomer, S., Driese, S. G., Lepland, A., Stinchcomb, G. E. & Kirsimäe, K. (2020), 'CO₂ drawdown and cooling at the onset of the great oxidation event recorded in 2.45 Ga paleoweathering crust', *Chemical Geology* p. 119678.
- [Svensen et al. (2009)] Svensen, H., Planke, S., Polozov, A. G., Schmidbauer, N., Corfu, F., Podladchikov, Y. Y. & Jamtveit, B. (2009), 'Siberian gas venting and the end-Permian environmental crisis', *Earth and Planetary Science Letters* **277**(3–4), 490–500.
- [Tilley et al. (2019)] Tilley, M. A., Segura, A., Meadows, V., Hawley, S. & Davenport, J. (2019), 'Modeling repeated M dwarf flaring at an earth-like planet in the habitable zone: atmospheric effects for an unmagnetized planet', *Astrobiology* **19**(1), 64–86.
- [Tolley (2018)] Tolley, A. (2018), 'Climate change and mass extinctions: Implications for exoplanet life', *Centauri Dreams*. <https://www.centauri-dreams.org/2018/12/14/climate-change-and-mass-extinctions-implications-for-exoplanet-life/>
- [Tsumura (2020)] Tsumura, K. (2020), 'Estimating survival probability using the terrestrial extinction history for the search for extraterrestrial life', *Scientific Reports* **10**(1), 1–9.
- [Von Paris et al. (2013)] Von Paris, P., Selsis, F., Kitzmann, D. & Rauer, H. (2013), 'The dependence of the ice-albedo feedback on atmospheric properties', *Astrobiology* **13**(10), 899–909.
- [Wagner et al. (2006)] Wagner, P. J., Kosnik, M. A. & Lidgard, S. (2006), 'Abundance distributions imply elevated complexity of post-paleozoic marine ecosystems', *Science* **314**(5803), 1289–1292.
- [Walker et al. (1981)] Walker, J. C. G., Hays, P. B. & Kasting, J. F. (1981), 'A negative feedback mechanism for the long term stabilization of Earth's surface temperature', *Journal of Geophysical Research* **86**(NC10), 9776–9782.
- [Wang & Stone (1980)] Wang, W.-C. & Stone, P. H. (1980), 'Effect of ice-albedo feedback on global sensitivity in a one-dimensional radiative-convective climate model', *Journal of Atmospheric Sciences* **37**(3), 545–552.
- [Way & Del Genio (2020)] Way, M. J. & Del Genio, A. D. (2020), 'Venusian habitable climate scenarios: Modeling Venus through time and applications to slowly rotating Venus-like exoplanets', *Journal of Geophysical Research: Planets* **125**(5), e2019JE006276.

[Wittmann & Pörtner (2013)] Wittmann, A. C. & Pörtner, H.-O. (2013), 'Sensitivities of extant animal taxa to ocean acidification', *Nature Climate Change* **3**(11), 995–1001.

[Wolf et al. (2018)] Wolf, E., Haqq-Misra, J. & Toon, O. (2018), 'Evaluating climate sensitivity to CO₂ across earth's history', *Journal of Geophysical Research: Atmospheres* **123**(21), 11–861.